Journal of Solid State Chemistry 184 (2011) 227–235

Contents lists available at ScienceDirect

Journal of Solid State Chemistry

journal homepage: www.elsevier.com/locate/jssc

Magnetic and transport properties of $RCr_{0.3}Ge_2$ (R=Tb, Dy, Ho and Er) compounds

A. Gil [a,*], D. Kaczorowski [b], B. Penc [c], A. Hoser [d], A. Szytuła [c]

[a] Department of Mathematics and Natural Science, J. Długosz University Częstochowa, Armii Krajowej 13/15, 42-200 Częstochowa, Poland
[b] Institute of Low Temperature and Structure Research, Polish Academy of Sciences, P.O. Box 1410, 50-950 Wrocław, Poland
[c] M. Smoluchowski Institute of Physics, Jagiellonian University, Reymonta 4, 30-059 Kraków, Poland
[d] BENSC, Helmholtz-Zentrum Berlin, Glienicker Str. 100, 14-109 Berlin, Germany

ARTICLE INFO

Article history:
Received 8 July 2010
Received in revised form
6 October 2010
Accepted 16 October 2010
Available online 23 October 2010

Keywords:
Rare-earth intermetallic compound
Neutron diffraction
Magnetic structure
Electrical properties

ABSTRACT

The magnetic and transport properties of ternary rare-earth chromium germanides $RCr_{0.3}Ge_2$ (R=Y and Tb–Er) have been determined. X-ray and neutron diffraction studies indicate that these compounds have the $CeNiSi_2$-type structure (space group *Cmcm*) [1]. Magnetic measurements reveal the antiferromagnetic ordering below T_N equal to 18.5 K (R=Tb), 11.8 K (Dy), 5.8 K (Ho) and 3.4 K (Er). From the neutron diffraction data the magnetic structures have been determined. For $TbCr_{0.3}Ge_2$ and $DyCr_{0.3}Ge_2$ at low temperatures the magnetic ordering can be described by two vectors $\mathbf{k_1}=(\frac{1}{2},0,0)$ and $\mathbf{k_2}=(\frac{1}{4},0,\frac{1}{4})$, and $\mathbf{k_1'}=(\frac{1}{2},0,0)$ and $\mathbf{k_2'}=(\frac{1}{2},0,\frac{1}{2})$, respectively. In $HoCr_{0.3}Ge_2$ and $ErCr_{0.3}Ge_2$ the ordering can be described by one propagation vector equal to $(\frac{1}{2},\frac{1}{2},0)$ and (0,0,0.4187(2)), respectively. In $DyCr_{0.3}Ge_2$ some change in the magnetic ordering is observed at T_t=5.1 K. In temperature range from T_t to T_N the magnetic ordering is given by one propagation vector $\mathbf{k}=(\frac{1}{2},0,0)$. $YCr_{0.3}Ge_2$ is a Pauli paramagnet down to 1.72 K which suggests that in the entire $RCr_{0.3}Ge_2$ series the Cr atoms do not carry magnetic moments. All compounds studied exhibit metallic character of the electrical conductivity. The temperature dependencies of the lattice parameters reveal strong magnetostriction effect at the respective Nèel temperatures.

1. Introduction

Rare-earth (R) ternaries of RT_xX_2 composition ($x \leq 1$), where T is a *d* element and X is a metalloid, form a large family of compounds with interesting magnetic properties which are presently being investigated by several authors (see references in [2]).

The $RCr_{0.3}Ge_2$ compounds investigated in this work belong to the germanides with T=*3d* elements. The germanides exist in stoichiometric (x=1) or nonstoichiometric ($0<x<1$) structures [3]. The magnetic and neutron diffraction data revealed complex magnetic properties of these compounds.

For $TbMn_{0.33}Ge_2$ the neutron diffraction data indicate a complex magnetic structure. In the temperature range 1.5–21 K the Tb magnetic moments have two components: a collinear antiferromagnetic G-type and a sine wave modulated while near the T_N=28 K new magnetic structure sinusoidally modulated is observed [4]. In $HoMn_{0.33}Ge_2$ at 4.2 K the collinear antiferromagnetic structure of G-type is observed [5]. Different magnetic properties are observed for $TbFe_xGe_2$. The compounds with x=0.25 have a monoclinic crystal structure and an antiferromagnetic ordering below T_N=20 K [6]. For compound with x=0.4 the neutron diffraction data detected an orthorhombic crystal structure and no magnetic ordering up to 1.57 K [7]. $HoFe_{0.33}Ge_2$ [8] and $ErFe_{0.3}Ge_2$ [9] order antiferromagnetically below 8 and 2.5 K, respectively.

The RCo_xGe_2 (R=Tb–Er) compounds with x=0.4–0.5 crystallize in the orthorhombic $CeNiSi_2$-type crystal structure. The Tb and Dy compounds have no magnetic ordering up to 1.5 K while these with R=Ho and Er are antiferromagnets with a collinear magnetic structure for R=Ho and a sine wave modulated for R=Er [10]. $TbNiGe_2$ is a G-type collinear antiferromagnet [11]. Also $TbNi_xGe_2$ with x=0.4 have similar type of magnetic ordering [12], while the phases with x=0.6 and 0.8 have complex magnetic structures with collinear G-type and sine modulated components [13]. $HoNi_{0.65}Ge_2$ (R=Tb, Ho and Er) have a G-type collinear magnetic structure [12,14].

The investigations of $RCr_{0.3}Ge_2$ compounds were first reported in Ref. [15]. The X-ray diffraction data indicated an orthorhombic crystal structure (space group *Cmcm*), and magnetic measurements showed that they are antiferromagnets with the Nèel temperatures equal 16.1 K (R=Tb), 9.9 K (Dy), 5.5 K (Ho) and 2.5 K (Er). For R=Tb and Dy compounds additional phase transitions were observed below the respective Neel temperature.

This work reports the results of X-ray, neutron diffraction, magnetic and electrical resistivity measurements. From these investigations the magnetic properties including the magnetic structures were determined. The obtained results are compared

* Corresponding author.
E-mail address: a.gil@ajd.czest.pl (A. Gil).

0022-4596/$ - see front matter © 2010 Elsevier Inc. All rights reserved.
doi:10.1016/j.jssc.2010.10.026

with the data for other isostructural germanides RT_xGe_2 in purpose to determine the influence of the *3d* element (T) on the magnetic properties.

2. Methods of investigation

Polycrystalline samples of $RCr_{0.3}Ge_2$ (R=*Y*, Tb, Dy, Ho and Er) were synthesized by arc melting the high-purity elements (R: 99.9 wt%; Cr: 99.9 wt% and Ge: 99.999 wt%) in titanium-gettered argon atmosphere. Afterwards, the samples were annealed in evacuated quartz ampoules at 800 °C for one week.

The samples were examined by X-ray powder diffraction performed at room temperature on a Philips PW-3710 X'PERT diffractometer using Cu$K\alpha$ radiation.

The magnetic data were collected within the temperature range 1.72–400 K and in external magnetic fields up to 5 T, using a Quantum Design MPMS-5 SQUID magnetometer. The electrical resistivity was measured in the temperature interval 3.8–280 K using a standard *dc* four-point technique.

The neutron powder diffraction patterns were collected at temperatures ranging from 1.5 to 25 K on the diffractometer installed at the BERII reactor (BENSC, Helmholtz Zentrum Berlin). The incident neutron wavelength was 2.45 Å.

The X-ray and neutron diffraction data were analyzed using the Rietveld-type program FullProf [16].

3. Results

3.1. Crystal structure

The X-ray diffraction data collected at room temperature (Fig. 1) as well as the neutron diffraction data recorded in paramagnetic state unambiguously confirmed that the investigated compounds crystallize in the orthorhombic $CeNiSi_2$-type crystal structure [1]. In this unit cell all the atoms are located at the 4(c) sites $(0,y_i,\frac{1}{2})$ with different values of the positional parameter y_i for R, Cr, Ge1 and Ge2 atoms. The values of the lattice parameters, the free positional parameters y_i and the occupancies of Cr atoms sites refined from the neutron diffraction data are listed in Table 1. The obtained parameters are in good agreement with the previous data [15]. In particular, the Cr atom statistically occupies one crystallographic position. Careful inspection of the X-ray and neutron diffraction intensities did not reveal any obvious additional reflections. This finding seems to exclude the monoclinic type structure reported for $TbFe_{0.25}Ge_2$ [6].

3.2. Magnetic behavior

The magnetic data of $RCr_{0.3}Ge_2$ (R=Tb–Er) compounds are shown in Fig. 2, and the main characteristics are summarized in Table 2. The compounds exhibit paramagnetic behavior from 400 K down to relatively low temperatures. The reciprocal magnetic susceptibilities, measured in a magnetic field of 0.1 T, obey the Curie–Weiss law with negative values of the paramagnetic Curie temperature θ_p and the effective magnetic moments μ_{eff} being close to the free R^{3+} ion values (see Table 2). At low temperatures, the magnetic susceptibility maxima typical for transitions into antiferromagnetic state are observed. The respective Nèel temperatures, defined as the position of the maximum in $\chi(T)$, are listed in Table 2. For $DyCr_{0.3}Ge_2$ an additional anomaly is observed at 5.1 K. In case of $TbCr_{0.3}Ge_2$ a small feature seen at 2.1 K is probably due to some amount of Tb_2O_3 impurity.

The antiferromagnetic ordering in the studied compounds is corroborated by the behavior of the isothermal magnetization taken at 1.7 K as a function of the external magnetic field. In each case a metamagnetic-like transition is observed in fields of 1 − 2 T. The values of the magnetic moment measured at T=1.72 K in the field H=5 T are much smaller than the respective free R^{3+} ion values (see Table 2), mainly because of crystal electric field effect. As is apparent from the table, our data are in good agreement with those reported in Ref. [15].

The temperature dependence of the magnetic susceptibility of $YCr_{0.3}Ge_2$ is displayed in Fig. 3. It is typical for Pauli paramagnets, and the upturn at low temperatures is likely due to some little admixture of unidentified impurities with stable magnetic moments. The field dependence of the magnetization taken at 1.72 K corroborates such interpretation.

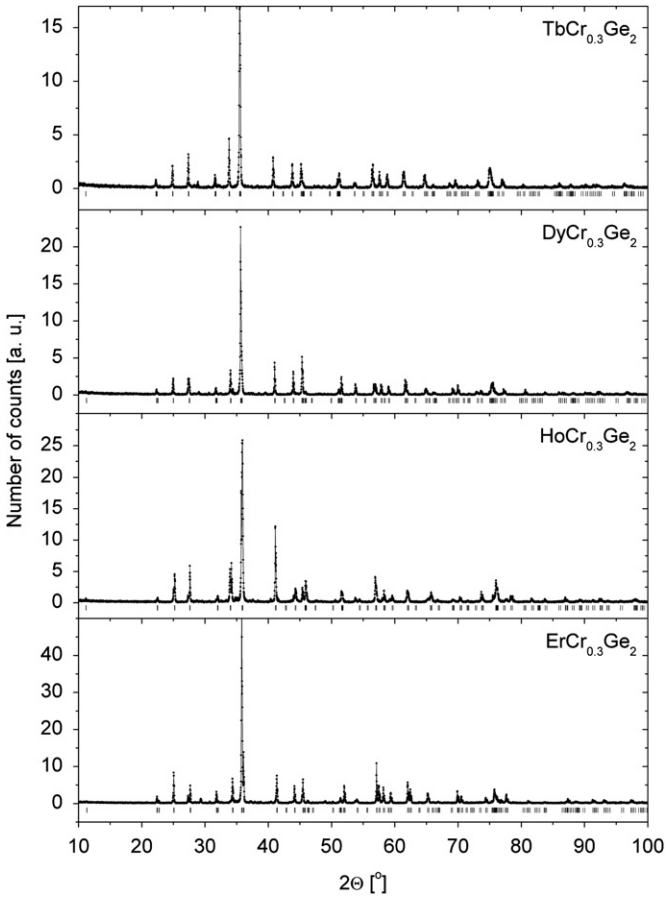

Fig. 1. X-ray diffraction patterns of $RCr_{0.3}Ge_2$ collected at room temperature.

Table 1
Values of the lattice parameters a, b and c, the unit cell volumes V, the positional atom parameters y_i and the occupancy of Cr site for $RCr_{0.3}Ge_2$ (R=Tb, Dy, Ho and Er) compounds, derived from the neutron diffraction data collected at different temperatures.

R	Tb	Dy	Ho	Er
T (K)	25	15	5.05	5
a (Å)	4.1529(6)	4.1435(6)	4.0957(9)	4.1180(9)
b (Å)	15.9780(24)	15.8853(26)	15.8998(34)	15.7090(42)
c (Å)	4.0249(7)	4.0203(6)	3.9602(10)	4.0035(9)
V (Å^3)	267.07(13)	264.62(12)	257.88(17)	258.98(19)
Occupancy	0.316(29)	0.328(30)	0.301(24)	0.316(24)
y_R	0.3954(7)	0.4002(6)	0.3973(9)	0.3964(6)
y_{Cr}	0.2150(36)	0.2135(39)	0.2095(44)	0.2172(30)
y_{Ge1}	0.0487(4)	0.0477(11)	0.0511(5)	0.0499(4)
y_{Ge2}	0.7492(5)	0.7461(8)	0.7498(7)	0.7500(5)
R_{Bragg} (%)	8.97	10.9	5.93	9.98
R_{prof} (%)	5.82	7.22	5.45	7.23

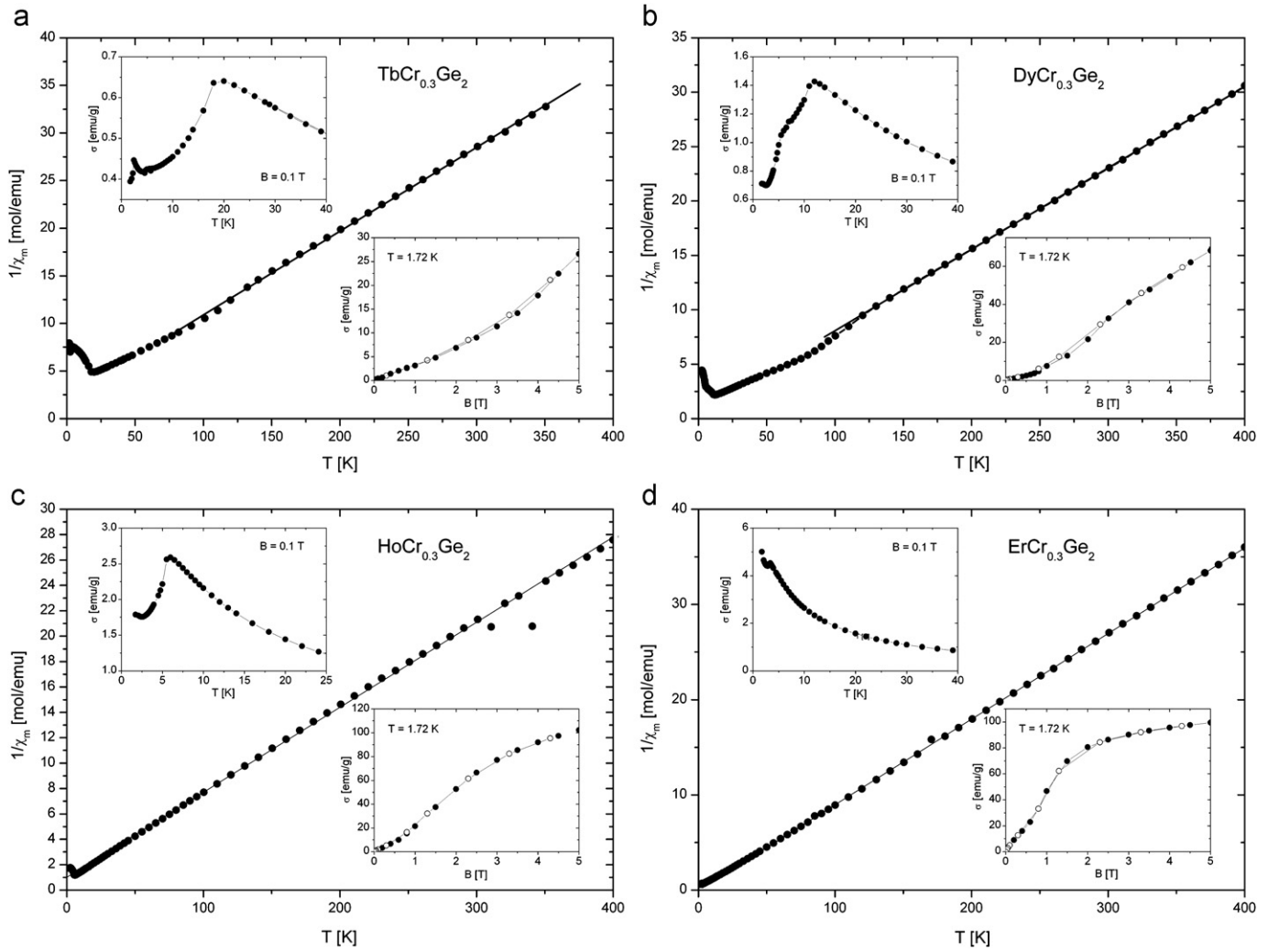

Fig. 2. Temperature dependence of inverse magnetic susceptibility χ^{-1} of $TbCr_{0.3}Ge_2$ (a); $DyCr_{0.3}Ge_2$ (b); $HoCr_{0.3}Ge_2$ (c) and $ErCr_{0.3}Ge_2$ (d). The solid lines represent the Curie–Weiss fit. The upper insets show a low temperature part of $\chi(T)$. The lower insets display the isothermal magnetization σ measured as a function of increasing and decreasing magnetic field B (closed and open symbols, respectively).

Table 2
Magnetic data for $RCr_{0.3}Ge_2$ (R=Tb, Dy, Ho, Er) compounds.

R	T_N (K) from		θ_p (K)	μ_{eff} (μ_B)		μ_s (μ_B)			Ref.
	$\chi(T)$	ND		Exp	Theor	Exp (M)	Exp (ND)	Theor	
Tb	18.5	18.2	−23.7	9.57		1.50	7.60(5)+4.52(7)		*
	16.1		−9.0(2)	9.73(1)	9.72	2.8		9.0	[3]
Dy	11.8	–	−7.93	10.38		4.0	7.18(12)+4.46(9)		*
	11.2		+4.5(2)	10.76	10.65	5.4		10.0	[3]
Ho	5.8	5.6	−15.0	10.97		6.07	6.99(6)		*
	6.4		−2.3(2)	11.08(1)	10.61	7.7		10.0	[3]
Er	3.4	3.5	+0.42	9.47		5.83	8.32(6)		*
	3.1		16.6(3)	9.67(1)	9.58	8.0		9.0	[3]

*—this work, ND—neutron diffraction, M—magnetization.

3.3. Electrical resistivity

The results of electrical resistivity measurements of $RCr_{0.3}Ge_2$ are presented in Fig. 4. All the compounds exhibit metallic-like conductivity. For the Tb-, Dy- and Ho-based phases one observes weak anomalies at low temperatures, which are due to the magnetic ordering. In the high temperature region where the magnetic contributions to the electrical resistivity may be assumed to be temperature independent, the resistivity data can be described using the Bloch–Grüneisen–Mott (BGM) formula

$$\rho(T) = (\rho_0 + \rho_0^{\infty}) + 4RT\left(\frac{T}{\theta_D}\right)^4 \int_0^{\theta_{D/T}} \frac{x^5 dx}{(e^x - 1)(1 - e^{-x})} - KT^3 \quad (1)$$

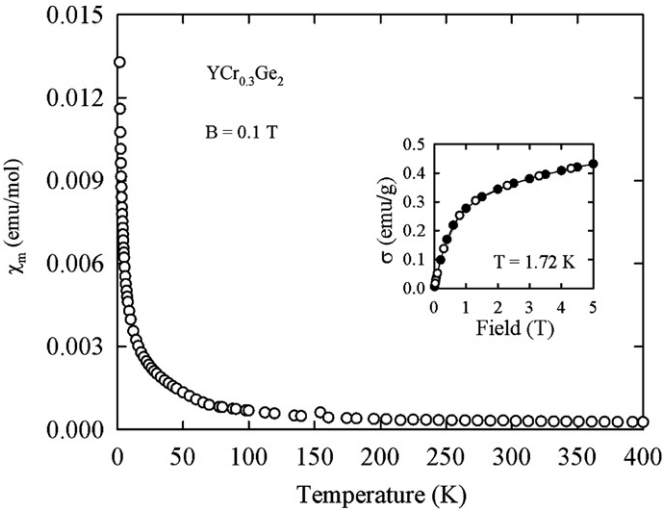

Fig. 3. Temperature dependence of the magnetic susceptibility of $YCr_{0.3}Ge_2$. The inset shows the isothermal magnetization σ measured as a function of increasing and decreasing magnetic field B.

The first term in this expression is a sum of the residual and spin-disorder resistivities ρ_0 and ρ_0^{∞}, respectively, the second term stands for the electron–phonon scattering process (θ_D is an estimate for the Debye temperature [17]), while the last one describes s–d interband scattering of conduction electrons. Least-squares fitting Eq. (1) to the experimental data (see the solid lines in Fig. 4) gives the parameters collected in Table 3. The values of $(\rho_0+\rho_\infty)$ are relatively large and this is likely a result of the presence of atomic disorder on Cr atom sites (partial occupancy). The values of the other parameters are of magnitudes typical for intermetallics. As might be expected, the derived Debye temperatures have similar values thus implying similar phonon spectra in all studied compounds.

3.4. Magnetic structures

Figs. 5, 7, 8 and 10 present the neutron diffractograms collected for the antiferromagnetic $RCr_{0.3}Ge_2$ (R=Tb, Dy, Ho and Er, respectively) ternaries. Comparisons of the diffraction patterns taken at low temperatures with those measured in the paramagnetic state clearly reveal the presence of some additional reflections due to the magnetic ordering. In the following, the neutron results are discussed separately for each compound.

The refinements of the experimental data have been undertaken considering the possibility of different moment arrangements given in Ref. [13].

3.4.1. $TbCr_{0.3}Ge_2$

In the neutron diffraction pattern collected at 1.5 K (Fig. 5) the additional peaks of magnetic origin form two groups. The first one, with strong intensities, can be indexed by the propagation vector $\mathbf{k}=(\frac{1}{2},0,0)$, while the second one, with small intensities, can be described by the propagation vector $\mathbf{k}=(\frac{1}{4},0,\frac{1}{4})$. The analysis of the magnetic peak intensities indicates that the Tb magnetic moments located at the positions Tb1 $(0,y,\frac{1}{4})$, Tb2 $(0,-y,\frac{3}{4})$, Tb3 $(\frac{1}{2},\frac{1}{2}+y,\frac{1}{4})$ and Tb4 $(\frac{1}{2},\frac{1}{2}-y,\frac{3}{4})$ form a collinear structure with the $(+\ +\ -\ -)$ sequence in the crystallographic unit cell for the first component (Fig. 6a) and $(-\ +\ +\ -)$ for the second one (Fig. 6b). For the first component, the Tb moment equal to 7.60(5) μ_B is parallel to the c-axis, whereas for the second component it amounts to 4.52(7) μ_B and forms an angle of 25(8)° with the c-axis. The magnetic structure corresponding to the first component consists of the ferromagnetic (1 0 0) planes with antiferro- or ferromagnetic coupling between the adjacent planes. The residuals for the two sublattices are $R_{mag}(1)=7.5\%$ and $R_{mag}(2)=16.7\%$.

The temperature dependencies of the magnetic moments (see Fig. 7) indicate that both magnetic phases are stable up to the Nèel temperature equal to 18.2 K. Remarkably, at the onset of the antiferromagnetic state the orthorhombic lattice parameters of $TbCr_{0.3}Ge_2$ exhibit distinct singularities. The neutron diffraction data have not revealed any change in magnetic structure near 2.5 K. The small peak in the temperature dependence of the magnetic susceptibility is probably connected with the Tb_2O_3 impurity. Such a peak was also observed in $\chi(T)$ for $TbFe_xGe_2$ (x=0.25 and x=0.4) [6] and $TbCo_{0.5}Ge_2$ [10].

3.4.2. $DyCr_{0.3}Ge_2$

The neutron diffractograms collected for $DyCr_{0.3}Ge_2$ (Fig. 8) reveal complex magnetic behavior with two components at 1.5 K. The first one can be described by the propagation vector $\mathbf{k}=(\frac{1}{2},0,0)$ (Fig. 9a). The Dy magnetic moments are equal to 4.46(9) μ_B and are coupled antiferromagnetically with the sequence $(-\ +\ +\ -)$. They are canted from the c-axis by an angle $\theta=27(5)^\circ$ and an angle of 49(10)° from the a-axis. In turn, the other component can be represented by the propagation vector $\mathbf{k}=(\frac{1}{2},\frac{1}{2},0)$ (Fig. 9b). Here, the Dy moments amount to 7.18(12) μ_B and order with the sequence $(+\ +\ -\ -)$. They form an angle of 29(3)° with the c-axis and an angle of 46(10)° with the a-axis. The residuals for two sublattices are $R_{mag}(1)=15.0\%$ and $R_{mag}(2)=14.2\%$.

At 6.5 K the magnetic ordering in $DyCr_{0.3}Ge_2$ involves only one propagation vector $\mathbf{k}=(\frac{1}{2},0,0)$. In this magnetic structure the Dy magnetic moments are equal to 5.96(5) μ_B. They are ferromagnetically coupled and for the angles $\theta=25(2)^\circ$ with the c-axis and 52(4)° with a-axis. The residual is $R_{mag}=11.3\%$.

3.4.3. $HoCr_{0.3}Ge_2$

The magnetic ordering in $HoCr_{0.3}Ge_2$ is described by the propagation vector $\mathbf{k}=(\frac{1}{2},\frac{1}{2},0)$. The observed zero intensity of the $(\frac{1}{2},\frac{5}{2},0)$ line on the neutron diffraction pattern collected at 1.5 K (Fig. 10) indicates the following arrangement of the magnetic moments $\mu_1=\mu_3=\mu_4=-\mu_2$. Such arrangement is in good agreement with the group theory analysis [8].

The Ho magnetic moment equal to 6.99(6) μ_B is aligned along the c-axis ($R_{mag}=7.9\%$). This type of magnetic ordering is stable up to the Nèel temperature of 5.6 K (see the inset of Fig. 10). As displayed in Fig. 11, the lattice parameters and the unit cell volume show clear magnetostrictive anomalies at the Nèel temperature.

The magnetic structure is depicted in Fig. 12. The structure may be viewed as a stacking of ferromagnetic slabs parallel to the (1 1 0) plane. These slabs are aniferromagnetically coupled with the adjacent ones along the stacking direction. The large intensity of the $(\frac{1}{2},\frac{1}{2},0)$ reflection should be related to the presence of the ferromagnetic (1 1 0) planes.

3.4.4. $ErCr_{0.3}Ge_2$

Fig. 13 presents the neutron powder diffraction patterns collected in the paramagnetic and ordered states of $ErCr_{0.3}Ge_2$. The diffractogram taken at 1.5 K reveals the presence of some additional reflections due to the magnetic ordering, which can be indexed by the propagation vector $\mathbf{k}=(0,0,0.4187(2))$. The Er magnetic moments are arranged in the sequence $(+\ +\ -\ -)$ at the Er1 $(0,y,\frac{3}{4})$, Er2 $(0,-y,\frac{3}{4})$, Er3 $(\frac{1}{2},\frac{1}{2}+y,\frac{1}{4})$ and Er4 $(\frac{1}{2},\frac{1}{2}-y,\frac{3}{4})$. The magnitude of magnetic moment is given by formula $\mu(\mathbf{r})=\mu_0\cos(2\pi\mathbf{kr})$, where μ_0 denotes the amplitude of modulation and $\mathbf{r}$ is a vector pointing from the beginning of the coordinates

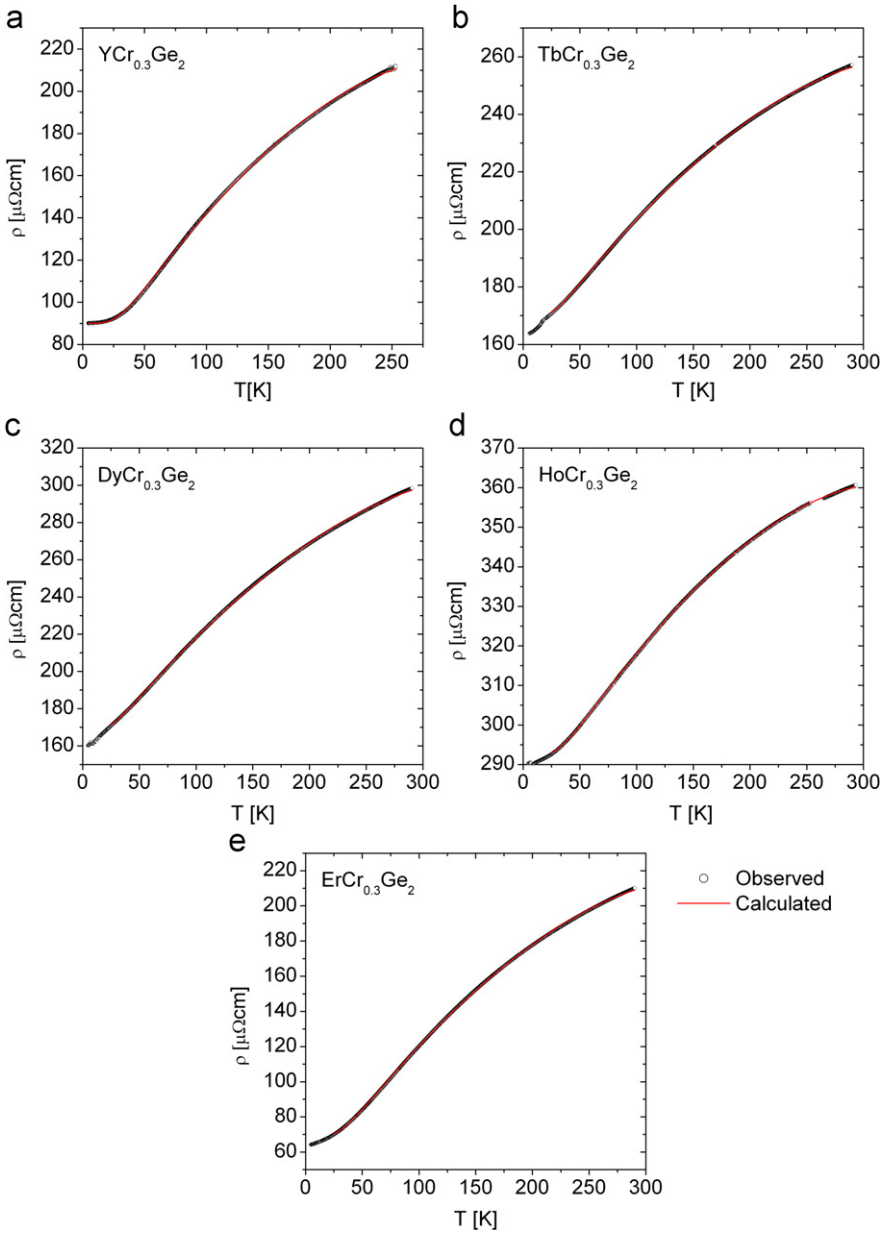

Fig. 4. Temperature dependence of the electrical resistivity ρ of $YCr_{0.3}Ge_2$ (a); $TbCr_{0.3}Ge_2$ (b); $DyCr_{0.3}Ge_2$ (c); $HoCr_{0.3}Ge_2$ (d) and $ErCr_{0.3}Ge_2$ (e). The solid lines represent the BMG fits to the experimental data, discussed in the text.

Table 3
Results of the analysis of the electrical resistivity data for $RCr_{0.3}Ge_2$ in terms of refinement of BMG model (see the text), as well as the ordering temperatures estimated from the temperature dependencies of $d\rho(T)/dT$.

R	T_N (K)	$\rho_0+\rho_\infty$ (μ Ωcm)	R (μ Ωcm K^{-1})	θ_D (K)	K (μ Ωcm K^{-3})
Tb	16.2	169.19(9)	0.3978(3)	160.6(1.2)	$1.17(1)\times10^{-6}$
Dy	8.3	168.50(11)	0.5730(4)	157.0(1.1)	$1.56(1)\times10^{-6}$
Ho	7.2	229.08(2)	0.3260(4)	197.5(4)	$1.07(1)\times10^{-6}$
Er	–	68.57(7)	0.6380(5)	191.8(6)	$1.80(1)\times10^{-6}$
Y	–	90.03(4)	0.6406(4)	185.0(4)	$2.46(1)\times10^{-6}$

systems. The derived value of μ_0 amounts 8.32(6) μ_B. The Er moment is parallel to the *a*-axis.

The magnetic structure is shown in Fig. 14. The Er moments form a chain along *c*-axis with the antiferromagnetic coupling along the chain and the ferromagnetic coupling between the adjacent (0 0 1) planes.

The Nèel temperature obtained from the temperature dependence of the magnetic reflection intensities is 3.5 K (see Fig. 15). As also shown in this figure, the k_z component of the propagation vector gradually decreases with increasing temperature. Alike, for the other $RCr_{0.3}Ge_2$ compounds the temperature dependencies of the lattice parameters *a*, *b* and *c* clearly indicate strong magnetostriction effect at the onset of the magnetically ordered state.

4. Discussion

The results for the $RCr_{0.3}Ge_2$ series presented in this work confirm the orthorhombic $CeNiSi_2$-type crystal structure and the antiferromagnetic ordering at low temperatures. The determined values of the respective Nèel temperatures are in good agreement with the previously published data [15]. For $DyCr_{0.3}Ge_2$ the neutron

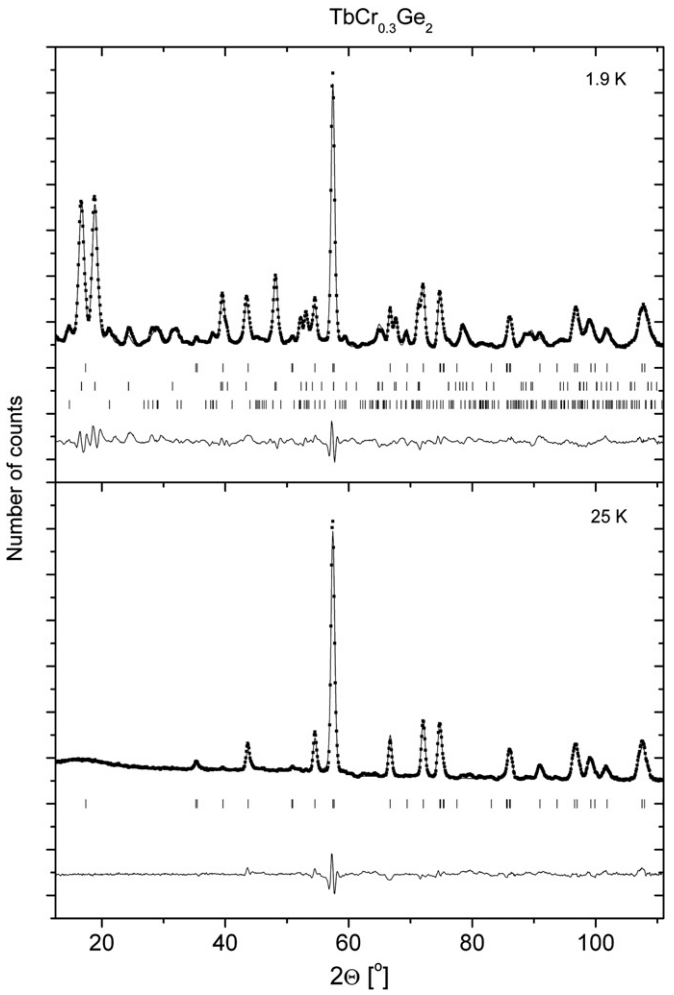

Fig. 5. Neutron diffraction patterns of $TbCr_{0.3}Ge_2$ collected at 1.5 and 25 K. The symbols represent the experimental data, and the solid lines are the calculated profiles for the crystal and magnetic structure models (see the text). The difference between the observed and calculated intensities is shown at the bottom of each diagram. The vertical bars indicate the positions of the Bragg peaks of nuclear (first row) and magnetic (second and third rows) origin.

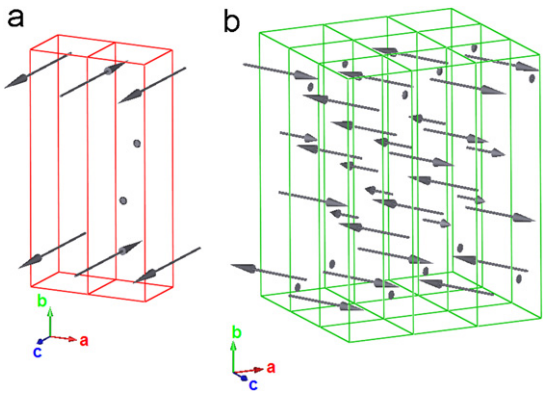

Fig. 6. Magnetic structure of $TbCr_{0.3}Ge_2$ at 1.5 K described by two propagation vectors $\mathbf{k}=(\frac{1}{2}, 0, 0)$ (a) and $\mathbf{k}=(\frac{1}{4}, 0, \frac{1}{4})$ (b).

diffraction data confirm the change of the magnetic structure. The key features of the established magnetic structures are as follows:

- $TbCr_{0.3}Ge_2$: in the temperature range between 1.5 K and T_N the magnetic order has two components with different propagation vectors and different orientations of the magnetic moments.
- $DyCr_{0.3}Ge_2$: at 1.5 K the magnetic order has two components with different propagation vectors, while at 6.5 K the magnetic structure is describable by a single component.
- $HoCr_{0.3}Ge_2$ and $ErCr_{0.3}Ge_2$: between 1.5 K and the respective T_N's the magnetic order can be described by one propagation vector. In $HoCr_{0.3}Ge_2$ this vector corresponds to commensurate structure, while in $ErCr_{0.3}Ge_2$ it yields an incommensurate magnetic unit cell.
- the neutron diffraction data have not indicated any magnetic moment on the Cr atoms. This latter finding is confirmed by the non-magnetic behavior of $YCr_{0.3}Ge_2$.

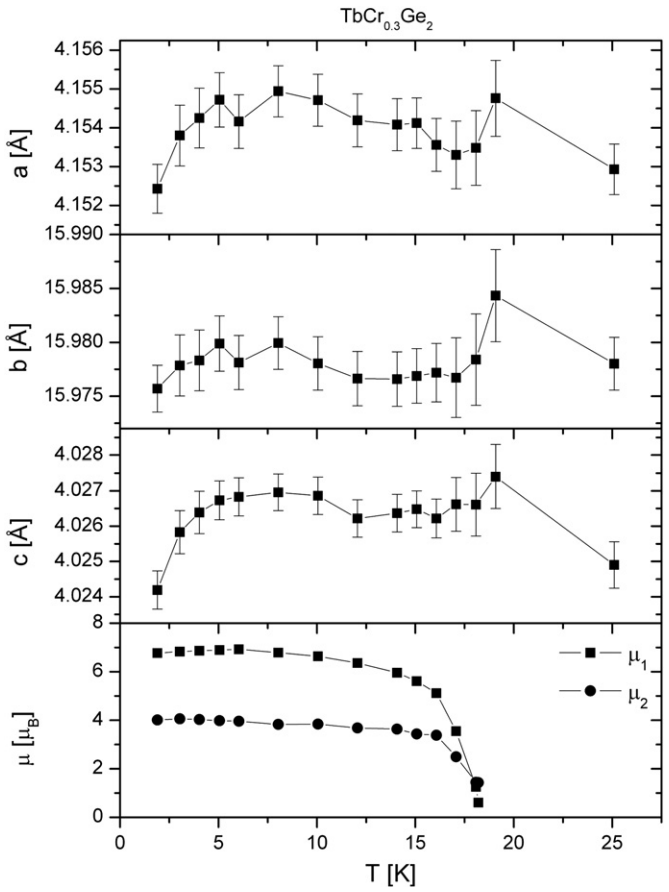

Fig. 7. Temperature dependencies of the lattice parameters a, b and c and the magnetic moments μ for $TbCr_{0.3}Ge_2$.

The magnetic structures determined for $RCr_{0.3}Ge_2$ are generally consistent with those reported for isostructural RT_xGe_2 compounds with T=Mn, Fe, Co, Ni and Cu [6–14]. The ternaries with the heavy rare-earth elements are antiferromagnets with collinear magnetic structures at low temperatures. In all compounds except those of the Mn-containing phases, the magnetic moments are localized on the rare-earth atoms only.

The magnetic ordering in $HoCr_{0.3}Ge_2$ appears very similar to those observed for $HoCo_{0.4}Ge_2$ [7] and $HoFe_{0.33}Ge_2$ [8]. In these compounds the antiferromagnetic arrangement along the [1 0 0] direction is observed, being describable by the propagation vector $\mathbf{k}=(\frac{1}{2},\frac{1}{2},0)$. In contrast, no such direct similarity is observed between the magnetic structures of $RCr_{0.3}Ge_2$ and those reported for RT_xGe_2 compounds with other d-electron transition metals.

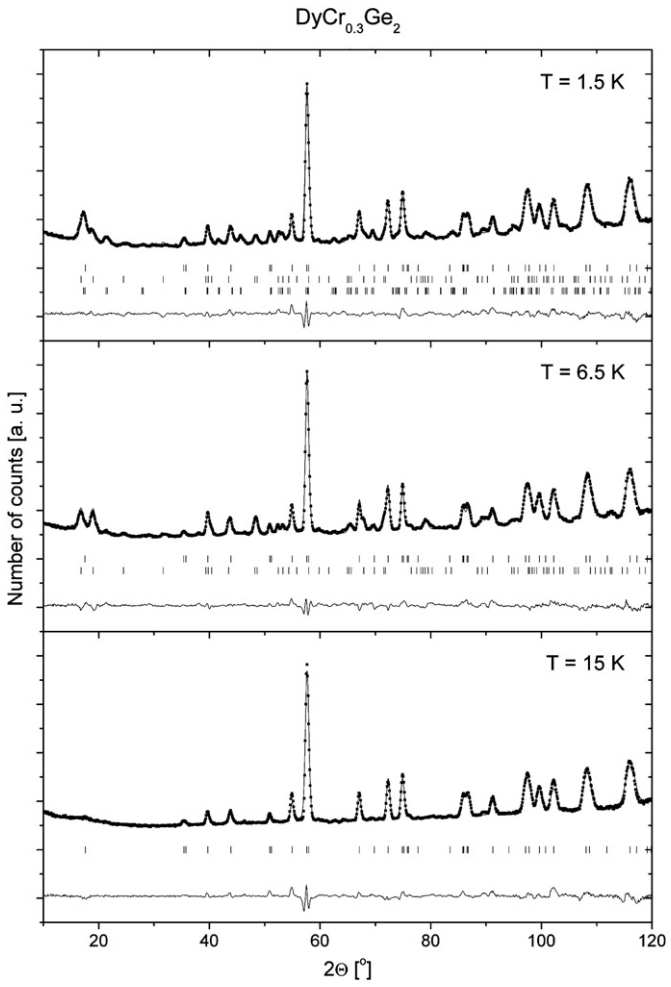

Fig. 8. Neutron diffraction patterns of $DyCr_{0.3}Ge_2$ collected at 1.5, 6.5 and 15 K (detailed description—see Fig. 5 caption).

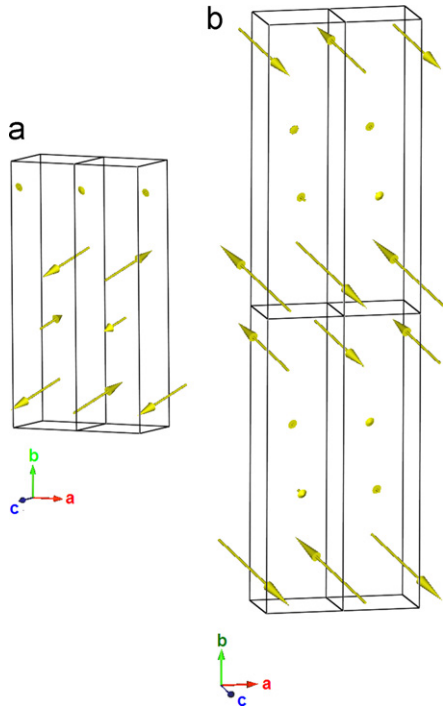

Fig. 9. Magnetic structure of $DyCr_{0.3}Ge_2$ at 1.5 K described by two propagation vectors $\mathbf{k}=(\frac{1}{2}, 0, 0)$ (a) and $\mathbf{k}=(\frac{1}{2}, \frac{1}{2}, 0)$ (b).

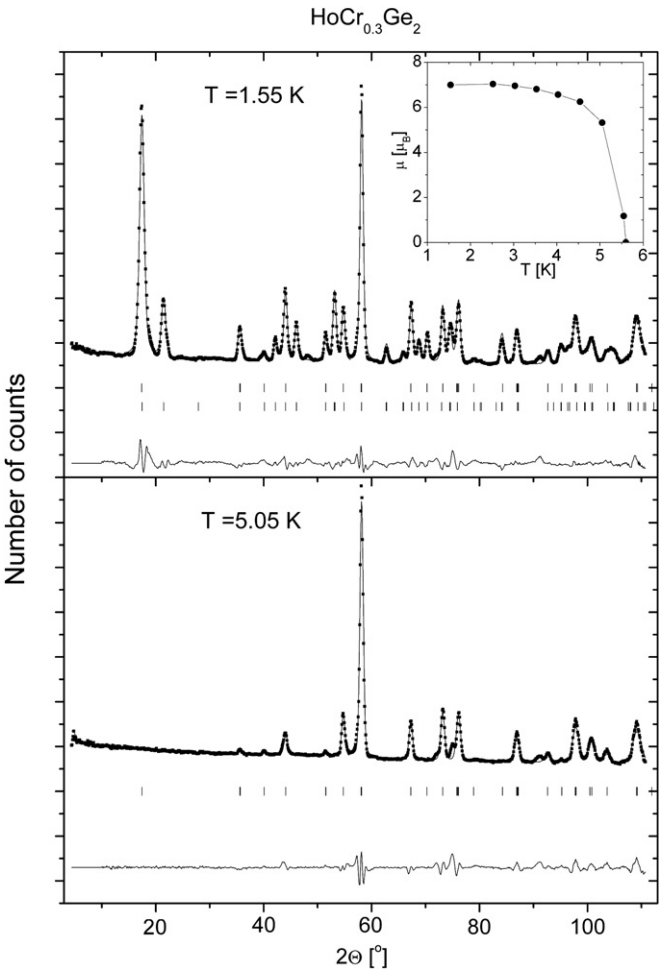

Fig. 10. Neutron diffraction patterns of $HoCr_{0.3}Ge_2$ collected at 1.55 and 5.05 K. The vertical bars indicate the positions of the Bragg peaks of nuclear (first row) and magnetic (second row) origin. The inset shows the temperature dependence of the Ho magnetic moment.

In general, the magnetic ordering in the studied compounds originates from interplay of exchange interactions between the magnetic moments localized on the rare-earth atoms, which are arranged in double-layer slabs stacked along the *b*-axis. The *R*–*R* distances within the slabs are near to 4.0 Å, whereas those between the slabs are ~5.5 Å. The rare-earth moments couple indirectly by spin polarization of conduction electrons (RKKY mechanism). The ordering temperature T_N decreases continuously on going from terbium to erbium. However, the expected scaling of the Nèel temperature with the de Gennes factor (see Fig. 6 in Ref. [15]) is not followed along the $RCr_{0.3}Ge_2$ series. The observed deviations can be attributed to the crystalline electric field effects (CEF).

Strong anisotropy in the magnetic coupling interactions connected with the distribution of the rare-earth atoms usually results in the formation of complex magnetic structures, especially if it is related to highly anisotropic arrangement of the atoms in the crystallographic unit cell. As an example it may be the complex magnetic structure determined for $TbCr_{0.3}Ge_2$, which involves two different wave vectors. Similar situations occur for isostructural $RNiSi_2$ (R=Dy,Er) and $TbNi_{0.6}Ge_2$ compounds [18–20]. In all these ternaries the magnetic ordering is the result of competing the long-range interactions of the RKKY-type between the rare-earth magnetic moments additionally influenced by CEF and likely also by small quadrupole–quadrupole interactions [21].

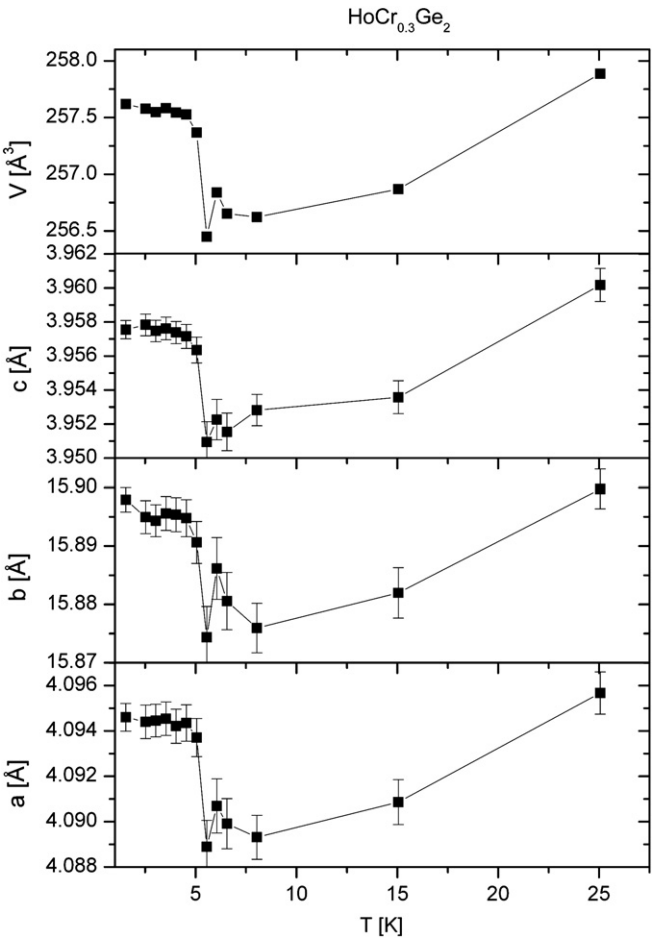

Fig. 11. Temperature dependencies of the lattice parameters *a*, *b* and *c* and the unit cell volume *V* for $HoCr_{0.3}Ge_2$.

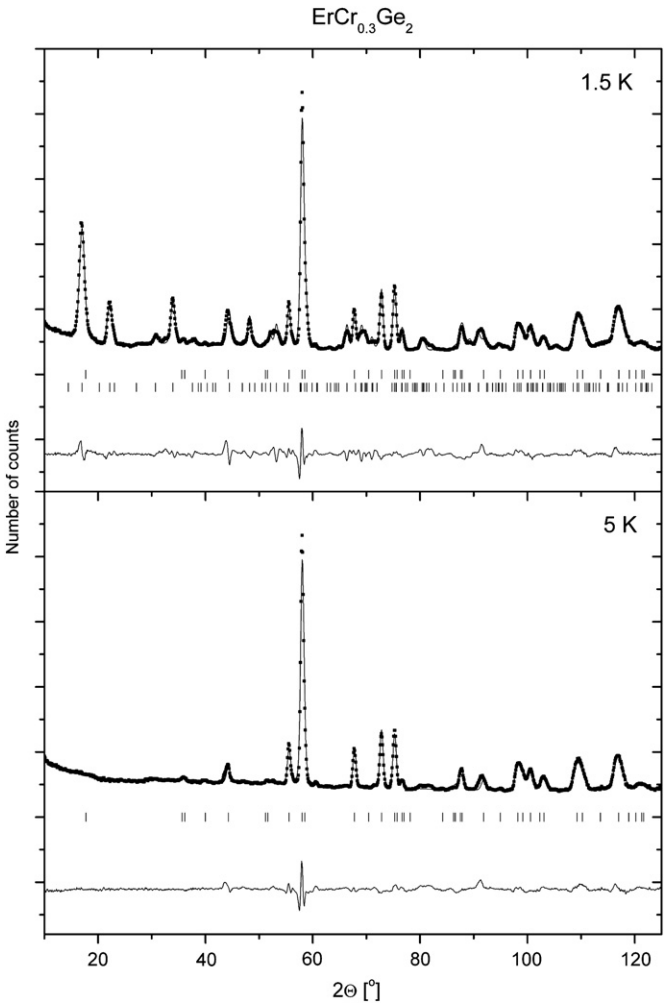

Fig. 13. Neutron diffraction patterns of $ErCr_{0.3}Ge_2$ collected at 1.5 and 5 K. The vertical bars indicate the positions of the Bragg peaks of nuclear and magnetic origin.

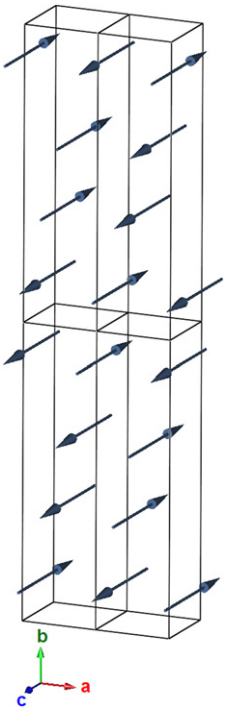

Fig. 12. Magnetic structure of $HoCr_{0.3}Ge_2$ at 1.5 K (propagation vector $\mathbf{k}=(\frac{1}{2}, \frac{1}{2}, 0)$).

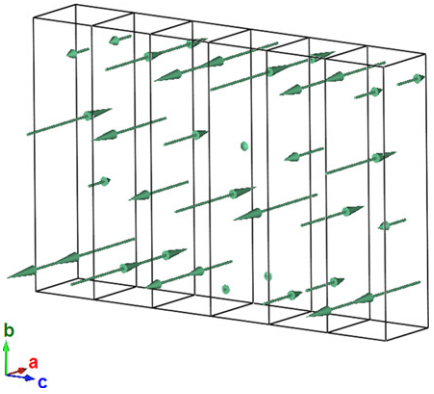

Fig. 14. Magnetic structure of $ErCr_{0.3}Ge_2$ at 1.5 K (propagation vector $\mathbf{k}=(0, 0, 0{,}4187)$).

The magnetic structures observed in $RCr_{0.3}Ge_2$, except for the R=Er are commensurate with the crystal structure. The rare-earth moments are parallel to the *c*-axis in $TbCr_{0.3}Ge_2$ and $HoCr_{0.3}Ge_2$ and slightly canted from this direction in $DyCr_{0.3}Ge_2$. On the contrary, in $ErCr_{0.3}Ge_2$ the magnetic moment is parallel to the *a*-axis. These results indicate that significant role is played by the CEF effects.

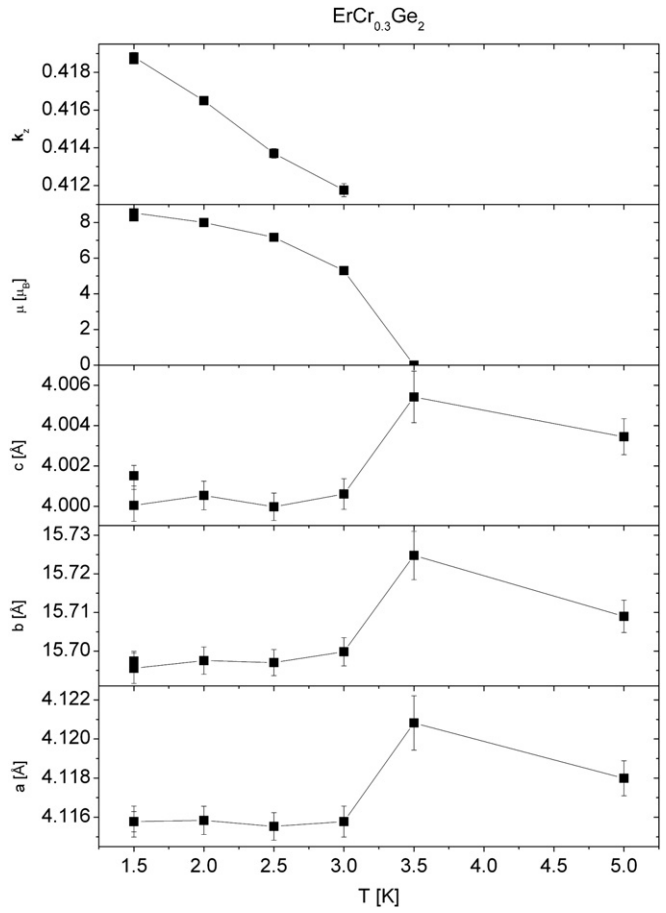

Fig. 15. Temperature dependencies of the k_x component of the propagation vector **k**, the values of the magnetic moment μ and the lattice parameters a, b, and c for $ErCr_{0.3}Ge_2$.

Changing the direction of the magnetic moments can likely be related to sign changes of the Stevens α_J coefficient from negative for R=Tb – Ho to positive for R=Er, Tm [22].

The metallic character of the temperature dependencies of the electrical resistivity is in good agreement with the high density of states on the Fermi level reported for $YFe_{0.25}Ge_2$ [6].

Acknowledgments

The work was supported by the European Commission under the 6th Framework Program through the key Action: Strengthening the European Research Area, Research Infrastructures Contract no. RII 3-CT-2003-505925 (NMI3).

References

[1] O.P. Bodak, E.I. Gladyshevskii, Kristallographie 14 (1969) 990–994.
[2] A. Szytuła, in: K.H.J. Buschow (Ed.), Handbook of Magnetic Materials, 6, 1991, p. 85.
[3] M. Francois, G. Venturini, B. Malaman, B. Roques, J. Less-Common. Met. 160 (1990) 197–213 and 215–228.
[4] A. Gil, M. Hofmann, B. Penc, A. Szytuła, J. Alloys. Compd. 320 (2001) 29–32.
[5] A. Gil, J. Leciejewicz, K. Małetka, A. Szytuła, Z. Tomkowicz, K. Wojciechowski, J. Magn. Magn. Mater. 129 (1994) L155–L159.
[6] M.A. Zhuravleva, D. Bilc, R.J. Pcionek, S.D. Mahantl, M.G. Kanatzidis, Inorg. Chem. 44 (2005) 2177–2188.
[7] S. Baran, D. Kaczorowski, B. Penc, D. Sheptyakov, A. Szytuła, J. Magn. Magn. Mater. 322 (2010) 2191–2194.
[8] S. Baran, Ł. Gondek, J. Hernandez-Velasco, D. Kaczorowski, A. Szytuła, J. Magn. Magn. Mater. 285 (2005) 188–192.
[9] B. Penc, A. Arulraj, D. Kaczorowski, A. Szytuła, E. Wawrzyńska, Acta Phys. Pol. A 117 (2010) 595–598.
[10] S. Baran, F. Henkel, D. Kaczorowski, J. Hernandez-Velasco, B. Penc, N. Stüsser, A. Szytuła, E. Wawrzyńska, J. Alloys Compd. 415 (2006) 1–7.
[11] W. Bażela, J. Leciejewicz, K. Małetka, A. Szytuła, J. Magn. Magn. Mater. 109 (1992) 305–308.
[12] P. Schobinger-Papamantellos, K.H.J. Buschow, J. Alloys Compd. 187 (1992) 73–80.
[13] A. Gil, B. Penc, J. Hernanez-Velasco, E. Wawrzyńska, A. Szytuła, J. Alloys Compd. 387 (2005) L8–L10.
[14] A. Gil, D. Kaczorowski, J. Hernandez-Velasco, B. Penc, E. Wawrzyńska, A. Szytuła, J. Alloys Compd. 384 (2004) L4–L6.
[15] H. Bie, A.V. Tkachuk, A. Mar, J. Solid State Chem. 182 (2009) 122–128.
[16] J. Rodriguez-Carvajal, Physica B 192 (1993) 55–69.
[17] J.M. Zunan (Ed.), 4th Ed., Claredon Press, Oxford, 1960 p. 412.
[18] P. Schobinger-Papamanthellos, K.H.J. Buschow, C. Ritter, J. Alloys Compd. 287 (1999) 51–56.
[19] P. Schobinger-Papamanthellos, C. Ritter, K.H.J. Buschow, J. Alloys Compd. 264 (1998) 89–94.
[20] P. Schobinger-Papamanthellos, K.H.J. Buschow, C. Wilkinson, F. Fauth, C. Ritter, J. Alloys Compd. 189 (1998) 214–224.
[21] R.J. Elliott, Phys. Rev. 124 (1961) 346–353.
[22] D. Gignoux, D. Schmitt, in: K.H.J. Buschow (Ed.), Handbook of Magnetic Materials, Vol. 10, Elsevier Science B.V., p. 239 (chapter 2) and references herein.